Pergamon

Cement and Concrete Research 33 (2003) 31–41

CEMENT AND CONCRETE RESEARCH

Microstructural study of sulfate attack on ordinary and limestone Portland cements at ambient temperature

E.F. Irassar*, V.L. Bonavetti, M. González

Department of Civil Engineering, National University of Buenos Aires Center State, Avenida Del Valle 5737, B7400JWI Olavarría, Argentina

Received 30 July 2001; accepted 26 June 2002

Abstract

This paper presents an investigation on the mechanism of sulfate attack on Portland cements (PCs) containing limestone filler. It is based on the analysis of microstructure and composition of mortar specimens (ASTM C 1012) stored for 2 years in sodium sulfate solution (0.352 M). Microstructure was studied using quantitative X-ray diffraction (XRD) on samples taken from the surface to the core of the specimens. The profile of compounds formed by sulfate attack was determined millimeter by millimeter at 1 and 2 years. Results show that sulfate attack in mortars containing limestone filler is characterized by an inward movement of the reaction front leading first to the formation of ettringite, later to gypsum deposition, and finally to thaumasite formation when the decalcification of mortar leads to the breakdown of C-S-H.

Keywords: Microstructure; X-ray diffraction; Sulfate attack; $CaCO_3$; Filler

1. Introduction

Modern cements often incorporate several mineral admixtures one of which is limestone filler. European standard EN 197 identifies two types of Portland limestone cements (PLC): Type II/A-L containing 6–20% and Type II/B-L containing 21–35%. In addition, the inclusion of 5% of filler material that can be calcareous is accepted in all cements. During 1990s, the Latin American countries also moved in this direction and the use of limestone filler in Portland cements (PCs) was standardized.

PCs exposed to sulfate environment can be damaged due to the formation of ettringite and gypsum. PLC can also be damaged by the formation of thaumasite because the presence of finely divided limestone could favor the formation of this compound in cold and very wet environment [1].

It is accepted that the reduction of the transport mechanism of aggressive sulfate ions is the main factor for improving the sulfate resistance of concrete [2]. However, low water-to-cement (w/c) should be adopted in combination with sulfate-resistant PC (SRPC) to prevent damages in very severe environments. Crammond and Halliwell [3] report that concretes containing limestone aggregates designed to provide a good sulfate resistance have suffered a particular type of sulfate attack in which thaumasite is formed. Consequently, it is very important to study the mechanism of sulfate attack in PCs containing limestone filler.

Results on sulfate performance of PCs containing limestone filler show different trends. Some authors [4–6] concluded that limestone filler could increase the sulfate resistance of cement, while other researches [7–9] found a decrease of sulfate resistance of this cement depending on the replacement level and clinker composition. In these studies, the experimental conditions varied widely. The solutions use different type of ions (Na_2SO_4 and $MgSO_4$), the concentration of solutions, the temperature of exposure, and the size of specimens vary widely. All these conditions influence the results obtained (expansion, strength, and weight loss), because sulfate attack is an external attack and it progresses slowly from the surface to the center of specimens. It can be pointed out that the course of sulfate attack is quite different depending on whether magnesium solution or sodium solu-

* Corresponding author. Tel.: +54-2284-451-055; fax: +54-2284-450-628.

E-mail address: firassar@fio.unicen.edu.ar (E.F. Irassar).

0008-8846/03/$ – see front matter © 2003 Elsevier Science Ltd. All rights reserved.
PII: S0008-8846(02)00914-6

tion is used. In the first case, magnesium sulfate appears to be more detrimental due to the conversion of CH to gypsum and brucite that leads to the breakdown of C-S-H [10]. When the expansion or strength is measured, the size of specimens has a decisive influence on the time to reach measurable damage [11,12]. The solution parameters are also important: its concentration [13], the pH value and whether the pH is controlled or not [14], and the temperature [15] favor some reactions or degradation processes.

Generally, thaumasite formation is identified in the degradation process of masonry mortar, historical building, and concrete in marine environment. The extended work of Gaze and Crammond [16] was made on masonry mortars, while the experiences reported by Ludwig and Mehr [17] on mortar (w/c = 0.70) containing PC or SRPC were made using an excess of gypsum, as in ASTM C 452 test. Then, both experiences expose the cement to condition rather different from the process of external sulfate attack to concrete.

Subsequently, a brief review on the performance of PLC exposed to a sulfate solution is presented. Hooton [18] has studied a low level of cement replacement by limestone filler (5%) in cement with high or moderate C_3A content using the ASTM C 1012 test. He concluded that the sulfate performance is only modified by the dilution effect. On the contrary, our studies [7,19] using the same test reveal that limestone filler addition decreases the sulfate resistance of moderate and low C_3A PC. In all cases, thaumasite was not found after 1 year. Tezuka et al. [20] report that mortar specimens ($40 \times 40 \times 160$ mm) containing 5–35% of various fillers (limestone, dolomite, and quartz) exposed to Na_2SO_4 solution showed no mass loss after 6 months.

Hartshorn et al. [8] report that the performance of paste containing 0%, 5%, 15%, and 30% of limestone filler exposed to cold (5 °C) solution becomes worse with increasing limestone addition and increasing concentration of $MgSO_4$ solution. They attributed this behavior to thaumasite formation.

Barker and Hobbs [21] have also studied the performance of PC and PC with 15% of limestone filler exposed to cold (5 °C) $MgSO_4$ solution (0.42%) and Na_2SO_4 sulfate (0.42%) using mortar prisms ($40 \times 40 \times 160$ mm). After 1 year, they concluded that the vulnerability to sulfate attack of mortars made with high C_3A PC and PLC cements was similar, although the mode of attack was different. Italian researchers [9] studied the performance of pastes and mortars with different PCs containing limestone filler exposed to cold (5 °C) $MgSO_4$ solution with different concentration (350, 750, and 3000 mg/l). After 5 years, paste and mortars with PLC showed a surface damage in the high concentrated solution due to the formation of thaumasite and ettringite. The damage was mitigated when an SRPC was used. However, they did not show loss of either compressive strength or elastic modulus.

Polish researchers [22] studied the expansion of concrete prisms ($50 \times 50 \times 150$ mm) after 1 year of storage in Na_2SO_4 solution (0.35 M). Their mixtures contained different amounts of limestone filler (0–28%) as sand replacement, a PC ($C_3A = 12.1\%$) with cement content of 350 kg/m^3, and different w/c ratios (0.50–0.70). They concluded that the addition of limestone powder to concrete improves its sulfate resistance.

The objective of this study is to identify the mechanism of sulfate attack in limestone filler cement and to understand the effect of limestone filler on mortar exposed to sodium sulfate solution. In addition, special attention is focused on the conditions under which thaumasite can be formed in sodium sulfate attack at ambient temperature.

2. Method and techniques

2.1. Specimens examined

Specimens ($285 \times 25 \times 25$ mm) were cast according to ASTM C 1012 (sand-to-cementitious material ratio of 2.75 and w/c of 0.485). After 24 h in a moist cabinet, they were removed from the mold and cured in saturated limewater until they achieved 30 ± 3 MPa compressive strength. At this age, the mortar bars were stored in individual plastic tanks containing Na_2SO_4 solution (0.352 M) for 2 years at room temperature (20 ± 2 °C). The pH of sulfate solution was periodically adjusted to 7 ± 1 and the consumption of titration solution, called sulfate demand, was registered as indicated in previous paper [7].

Mortar bars were prepared using normal PC with a mineralogical composition (Bogue) of $C_3S = 51\%$, $C_2S = 26\%$, $C_3A = 6\%$, and $C_4AF = 10\%$. The Blaine fineness of the PC was 285 m^2/kg. PLC (PLC10 and PLC20) were produced by mixing limestone filler (10% and 20% by weight) with PC. The limestone filler contained 85% of $CaCO_3$ and its Blaine fineness was 710 m^2/kg.

Complete experimental details and results of expansion, strength development, and sulfate demand for these specimens were reported in a previous paper [7]. In this paper, the evolution of the visual aspect and the microstructural study are the new data presented. The relationship of expansion and consumption of titration solution is also presented.

2.2. Obtaining compound profiles

Compound profiles formed during sulfate attack were determined at 1 and 2 years for all cements used. Mortar samples were obtained using a similar technique as that described by McGrath and Hooton [23], who determined the chloride profile millimeter by millimeter in concrete. After measuring the length and testing the flexural and compressive strength as indicated in a previous paper [7], the remaining slices were immersed in acetone to stop the hydration and then dried at 40 °C over a period of 7 days. Subsequently, using the wearing device, layers of 1-mm depth were obtained from the surface to the core of the

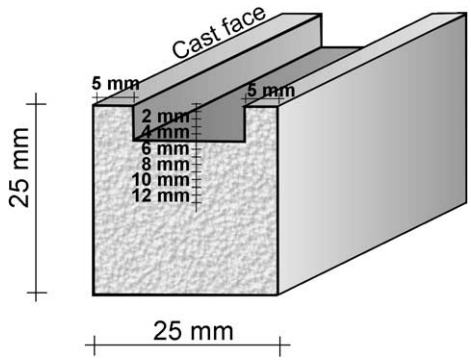

Fig. 1. Diagram of the profile sampling in mortar bars.

specimen. Material was obtained by cutting perpendicularly to the prism face at 5 mm from both edges of the prism (Fig. 1). The layer depth was selected at 1 mm because 100% of sand used in making the mortar passed through a 1.18-mm sieve (#16). The sample taken in this 1-mm layer is representative of the compounds formed both in paste and in the paste–aggregate interfaces.

The material from each layer was collected and sieved through a 75-μm sieve (#200) to remove the bulk of the sand grains. Finally, the sample was ground to pass through 45-μm sieve (#325) and stored in a desiccator to prevent carbonation before X-ray diffraction (XRD) analysis.

2.3. XRD analysis

XRD measurements were performed on Philips X'Pert diffractometer equipped with a graphite monochromator using CuKα radiation and operating at 40 kV and 20 mA. Step scanning was used with a scan speed of 2°/min and sampling interval of 0.02° 2θ.

Fig. 2 shows the XRD patterns at 2 years for PC and PLC20 mortars. In these diagrams, the quartz peaks were reduced using software to clearly show the compounds formed by sulfate attack.

Quantitative analysis was made by the integration of the area below the peaks of the compounds detected. Peak area was obtained by XRD resampling around 2θ deg peak and then calculated using the APD software. The peaks selected

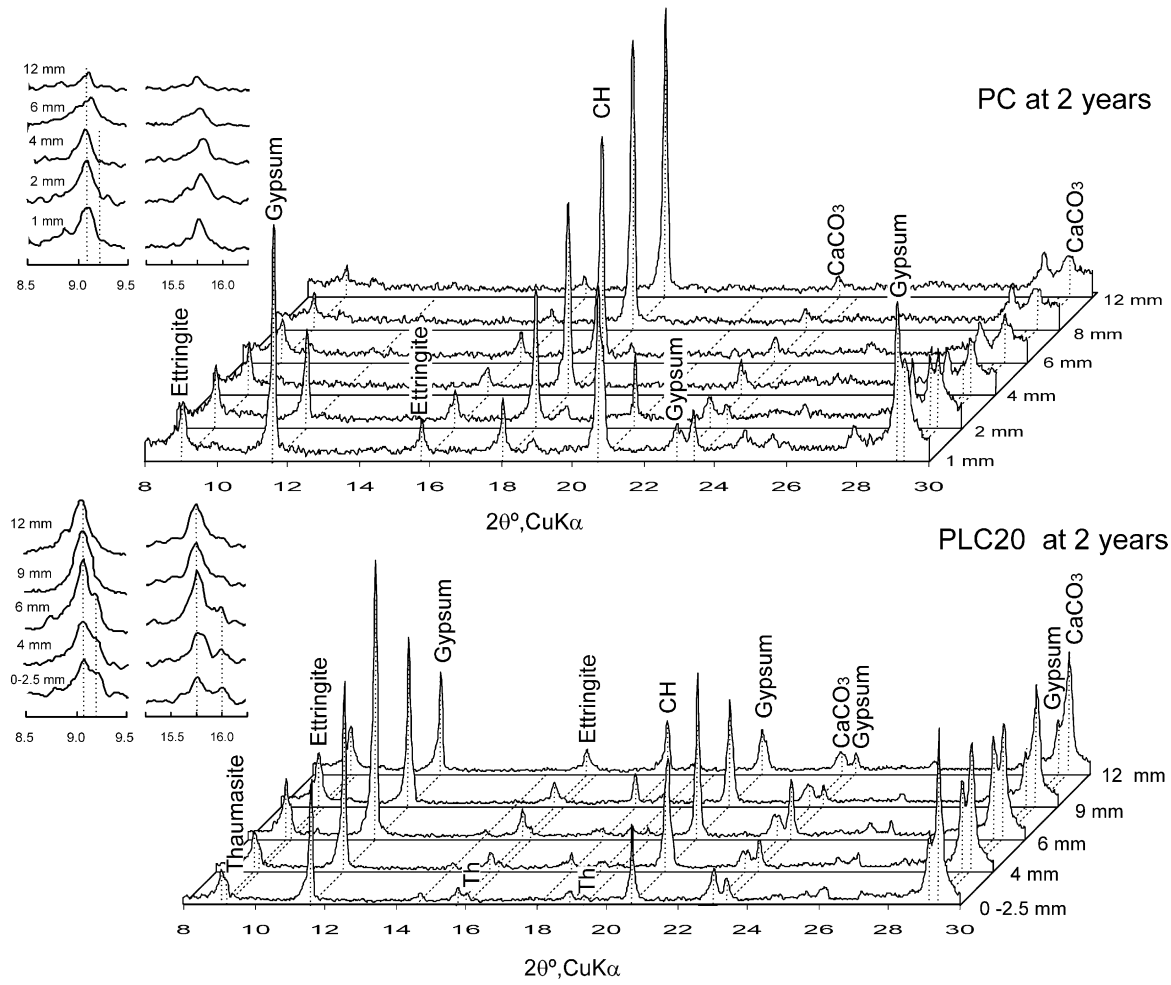

Fig. 2. XRD patterns at different depth for PC and PLC20 mortars exposed for 2 years in sodium sulfate solution.

to quantify these phases were ettringite at 9.08° 2θ, gypsum at 11.59° 2θ, CH at 18.04° 2θ, and $CaCO_3$ at 29.4° 2θ.

Ettringite and thaumasite are detectable by XRD [24]. However, the quantitative determination of these phases was not possible because their two main peaks (9.08° and 15.79° 2θ for ettringite and 9.15° and 16.0° 2θ for thaumasite, respectively) are very close due to the structural similarity of both compounds. However, the double peaks at 15.79° and 16.0° 2θ and deformation of the main peak (9.08° and 9.15° 2θ) are quite evident when the XRD pattern is enlarged (see detail in Fig. 2). Also, some small peaks can be used to identify the presence of either ettringite or thaumasite. In particular, the thaumasite peaks at 19.35° 2θ are absent in ettringite pattern. Likewise, there is an ettringite peak that has no equivalent in the thaumasite pattern at 22.96° 2θ but it is very close to the $CaCO_3$ peak corresponding to the limestone filler.

2.4. Scanning electron mmicroscopy (SEM)

Fragments of specimens broken off and washed with acetone were examined by SEM equipped with energy dispersed X-ray spectroscopy (EDS). This analysis was specially carried out to identify the ettringite and thaumasite crystals.

3. Results

3.1. Expansion and sulfate demand

Fig. 3 shows the relationship between expansion and the consumption of titration solution to adjust the pH of solution

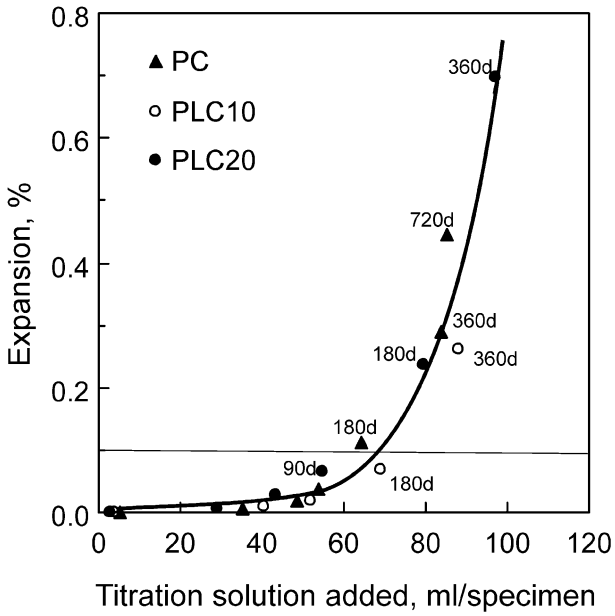

Fig. 3. Relationship between expansion and volume of titration solution added to maintain the pH.

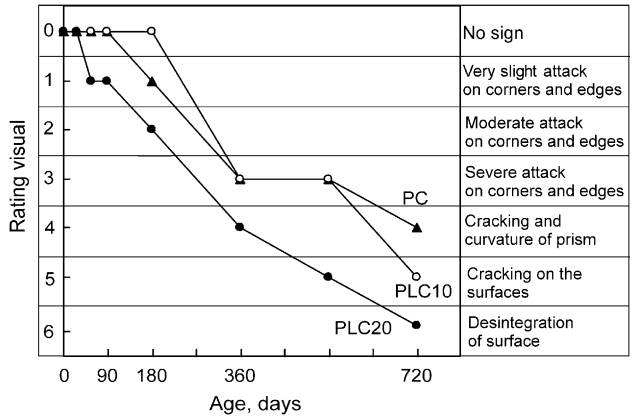

Fig. 4. Evolution of the progress of deterioration judged by visual appearance of mortar specimens.

(sulfate demand). At early exposure age, there was a large addition of titration solution to adjust the pH but the expansion was little for all cements. Subsequently, expansion increases with a moderate rate of sulfate demand. For these cements, the rate of expansion was different as reported previously [7], but it seems that the relationship of expansion to solution consumption was identical for all cements. This relationship indicated that sulfate attack of prisms has an initiation period during which SO_4^{2-} ions penetrate into the specimen causing little expansion. Finally, when the core of the specimens was attacked by sulfate, the expansion increased rapidly with a moderate sulfate demand. This is due to the fact that expansion is measured on the center axis of the prisms.

3.2. Visual appearance

Fig. 4 shows the progress of deterioration in terms of visual rating of mortar specimens. Results indicate that deterioration of PLC20 mortar was manifested after 56 days when small cracks appeared on corners. Subsequently, specimens expanded rapidly and they appeared with a large curvature at 1 year. At 2 years, specimens were severely damaged presenting surface softening (about 2.5 mm in depth), the mortar was reduced to a soft pulpy mass and it could be broken easily with the hand. On the contrary, the PC mortar bars required 180 days in sulfate solution to show the first visual sign of deterioration. At 2 years, they presented extensive cracks along their edges, but their cores were still intact. In the PLC10 mortar, specimens showed no sign of damage up to 1 year, then their deterioration rate increased rapidly, and they were completely cracked and exhibited a surface softening at 2 years.

3.3. Compound profiles

The distribution of products formed by the sulfate attack quantified by XRD is illustrated in Figs. 5–7 for PC,

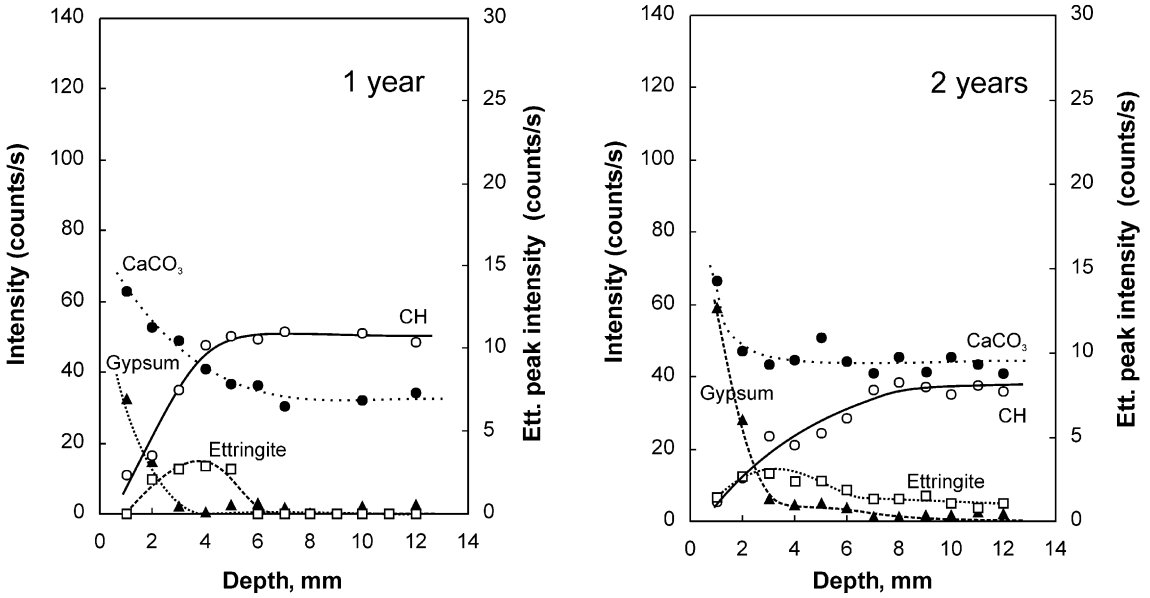

Fig. 5. Distribution of attack products quantified by XRD in PC mortar at 360 and 720 days of sulfate exposure.

PLC10, and PLC20 mortars, respectively. The results are commented in accordance with the criteria quoted by Wang [25]. This author defines the *sulfate attack transition zone* (SATZ) as the depth when the composition and the amount of hydration products have dramatically changed between that found at the surface and that found in the bulk material. In this zone, as shown in the profile figures, ettringite has a bell-shaped distribution from the surface to the core of specimens and there is a reverse relationship between the distribution of gypsum and CH. Gypsum has a maximum near the surface and it decreases rapidly to zero inside the specimen while the intensity of the CH peak increases from little to nil at the surface to a maximum at the center of the specimen. In the present investigation, the evolution of calcium carbonate was also included and its distribution increases from a maximum at the surface to a constant level at the center. This level represents the amount of limestone filler addition in the mortar.

3.3.1. PC mortar

For the PC mortar, Fig. 5 shows that the SATZ was bellow 4 mm at 1 year and was around 5 mm at 2 years. Ettringite was detected to about 5 mm in depth and the maximum of the bell shape was found at 3 mm at 1 year.

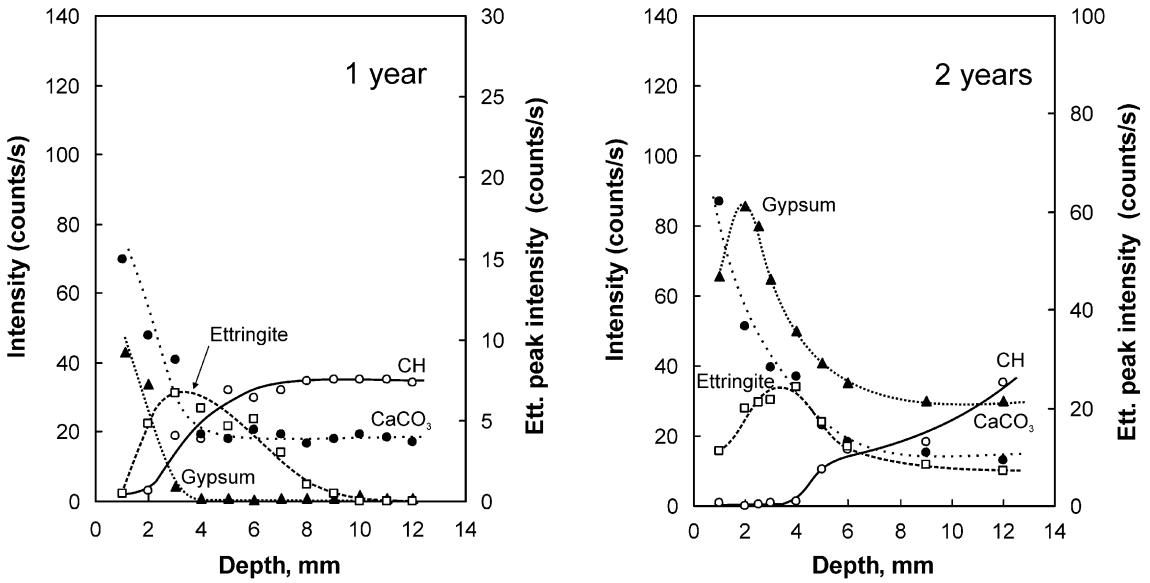

Fig. 6. Distribution of attack products quantified by XRD in PLC10 mortar at 360 and 720 days of sulfate exposure.

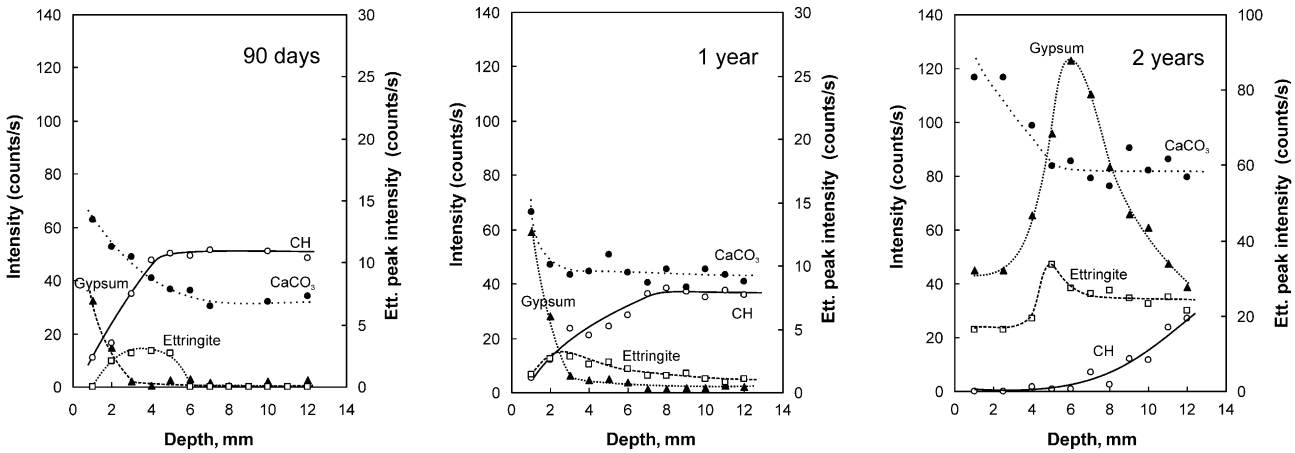

Fig. 7. Distribution of attack products quantified by XRD in PLC20 mortar at 90, 360, and 720 days of sulfate exposure.

Later, the amount of ettringite was similar between 1 and 6 mm in depth and the distribution curve did not show a maximum. However, ettringite was detected at the 12-mm depth indicating the progress of the attack into the mortar. At the outer layer of specimen, thaumasite was not found and the details of XRD pattern (Fig. 2) show no noticeable change in the main ettringite peak and the absence of double peak at 15.79–16.0° 2θ. The presence of gypsum accompanied with the depletion of CH at depth of 4 mm was observed at both studied ages. Calcium carbonate, formed by carbonation, was also detected in the SATZ.

The main difference between the profiles at 1 and 2 years was the depth where the ettringite was detected by the XRD analysis. However, the SATZ was similar in both profiles.

3.3.2. PLC10

The compound profile shows that the SATZ is located from the surface to 3–4 mm below at 1 year (Fig. 6). Ettringite was detected up to 10 mm from the surface and the maximum of the bell shape was found at 4 mm with a stronger intensity peak compared with the corresponding PC mortar. In the vicinity of the surface (1 mm layer), thaumasite peaks were not found. The profiles of gypsum and CH have the same shape as the PC mortar.

At 2 years, thaumasite was revealed by XRD at 1-mm depth. Thaumasite was identified by the deformation of the main ettringite peak, the double peaks at 15.79–16.0° 2θ, and its characteristic peak at 19.35° 2θ. At 2 mm below the surface, a slight deformation of the main ettringite peak was only detected. The maximum ettringite distribution was found at 4 mm and its peak intensity was four times stronger than that of the PC mortar. The peak intensity of this compound was almost similar from 6 mm in depth to the core of the specimen.

Up to 4 mm in depth, little or no CH was detected indicating its extreme depletion of CH. For this stage of deterioration, gypsum was detected across the whole section and its distribution also has a bell shape with a maximum near the surface. The amount of calcium carbonate decreased from a maximum at the surface to the amount of limestone content at 5-mm depth.

3.3.3. PLC20

The SATZ was 4 mm thick at 1 year, while the whole section was altered by sulfate attack after 2 years of exposure. For this mortar, a complementary profile at 90 days is presented in Fig. 7. It shows that ettringite was detected up to 5 mm in depth and the bell maximum was at 3–4 mm. Gypsum was also found with a declining intensity from the surface up to 3 mm and it was accompanied by consequent CH depletion. This observation corroborates that initial stages of attack were similar to the PC mortar.

At 1 year, the main ettringite peak was found at all the depths studied and its distribution presented a maximum at 3 mm. A slight deformation of the main peak of ettringite was observed at the 1- and 2-mm layers, but the double peaks at 15.79–16.0° 2θ were absent. Peak intensity was higher than in the PC mortar and lower than in the PLC10 mortar. Gypsum was detected up to 6 mm of depth and the reduction of CH was found at the same depth. The progress of carbonation is very low.

At 2 years, thaumasite was detected in the XRD pattern (9.15°, 16.0°, and 19.35° 2θ) on the sample obtained from the spalled zone (2.5 mm). It was also detected from 4 to 6 mm in depth (see detail in Fig. 2), but thaumasite was not be identified from the 7-mm depth to the center. Across the whole section, the amount of ettringite–thaumasite was four times higher in this sample than the maximum found in the PC mortar.

A dramatic change in the amount of CH was observed for this sample. CH was not detected from 0 to 6 mm in depth, and the amount quantified in the center of specimens was the half than the corresponding amount in PC mortar. Also, gypsum was present in the whole section and it had a bell-shaped distribution with a maximum at 6 mm in depth. From 0- to 4-mm depth, a decrease of the gypsum was observed while the calcium carbonate increases.

4. Discussion

Results presented here indicate that sulfate attack of PC and PLC mortars is a progressive phenomenon from the surface inwards and involves several stages. These data agree closely with the mechanism of sulfate attack proposed by Gollop and Taylor [26] and the early stages of attack reported by Wang [25], despite the fact that their works were done in PC pastes. Bonen [27] has demonstrated that the course of sulfate attack is different in mortars or concrete compared with cement paste due to the presence of aggregate, which leads to a higher porosity at the interface between paste and aggregate.

Based on the results reported in the literature and presented in this paper, the sequence of attack is schematically illustrated in Fig. 8 and it has the following stages: (1) diffusion of SO_4^{2-} and CH leaching, (2) ettringite formation, (3) gypsum formation and depletion of CH, (4) decalcification of C-S-H, and (5) thaumasite formation. This sequence of reaction in both PC and PLC mortars is the same as reported previously [7].

4.1. Diffusion of SO_4^{2-} and CH leaching

At early ages, the high amount of titration solution needed to maintain the pH is related to the leaching of CH from the specimen surfaces [14] and later it is related to the progress of the sulfate diffusion process.

In the PC mortar, the consumption rate decreases with time. Consequently, the mortar solution system reaches equilibrium. This process involves a two-counter-ion flow: the $(OH)^-$ and Ca^{2+} diffuse from inside the mortar to the solution and the SO_4^{2-} diffuse from the solution to the mortar [26,28]. The $(OH)^-$ are derived mainly from the dissociation of CH that is highly soluble at pH of 7 ± 1. The intensity of this ion flow depends on the porosity of the mortar, the changes in porosity caused by the sulfate attack and the concentration gradient [29]. In an uncontrolled pH environment, Gollop and Taylor [30] also found an increase of Ca^{2+} concentration in the sulfate solution.

All the time, PLC20 mortar had a higher rate of consumption of titration solution than PC mortar [7]. Analyzing the depth of SATZ at 2 years, it can be observed that the penetration of SO_4^{2-} was more pronounced for PLC20 mortar than that of PC mortar.

4.2. Ettringite formation

Ettringite is formed by the reaction of SO_4^{2-} with the AFm phase (i.e., monosulfoaluminate and monocarboaluminate) present in mortar. According to Gollop and Taylor [30], ettringite at early stages of attack is mixed within the C-S-H on a scale too fine for resolution by XRD, while the ettringite detected by XRD is a well-crystallized compound that forms in cracks or voids. Ettringite can also be formed as a result of reaction between SO_4^{2-} and the ferroaluminate phase [26,31].

Several researches [6,22,32] focused their conclusions about sulfate performance of PLC on the stability of the aluminate hydrates forming prior to sulfate immersion. In PC, the conversion of primary ettringite to monosulfoaluminate might be expected. On the other hand, the presence of limestone in mortars suppresses or delays the conversion of ettringite to monosulfoaluminate and, instead, the monocarboaluminate is formed [33,34]. In addition, some amount of ettringite is preserved with their crystallization [34–36]. However, XRD analyses of PLC10 and PLC20 mortars reveal the formation of ettringite after sulfate immersion. This could have originated as results of the transformation of the AFm phase that was not detected by XRD before the immersion. The contribution that of the part of the aluminates that remains crystallized as ettringite (a stable compound in sulfate environment) due to the monosulfoaluminate decomposition by carbonate ions [33,34] appears not to be significant for the sulfate performance of these cements.

XRD analyses show that ettringite crystals grow after sulfate immersion at the surface of mortar. It was observed by SEM mainly in void pores, but it cannot be detected within the paste or transition zone. Gollop and Taylor [30]

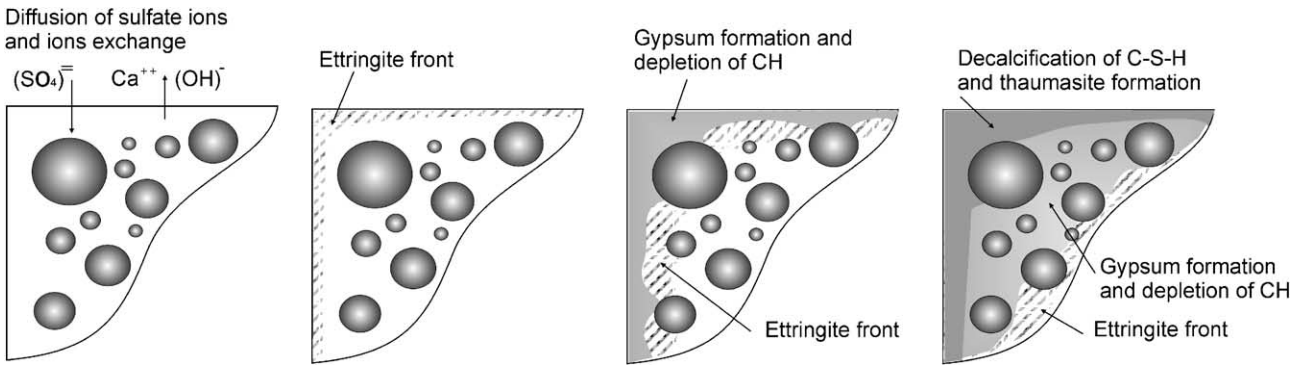

Fig. 8. Schematic representation of the sequence of sulfate attack in mortar.

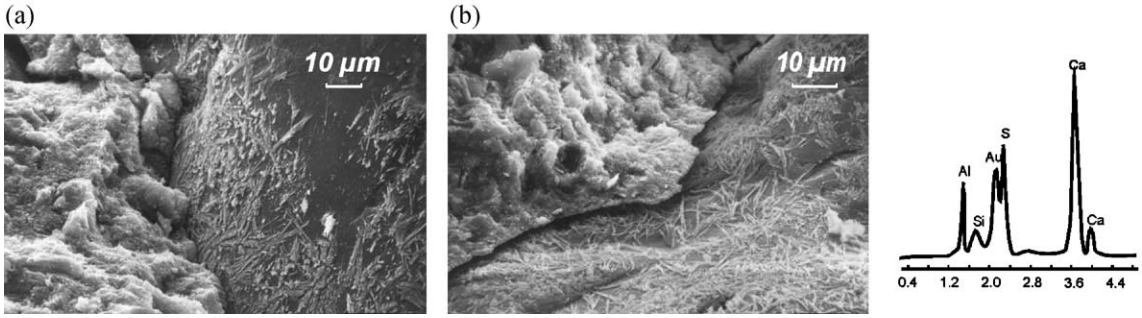

Fig. 9. SEM photographs of ettringite at paste–aggregate interface of (a) PLC10 mortar at 2 years (b) PLC20 mortar at 1 year.

suppose that the crystals that grow within the cement gel have submicroscopic dimensions causing forces that disrupt the structure of the paste leading to cracking. XRD profiles corroborate that ettringite is the first attack product detected in the surface at early ages and that it is the vanguard of the attack front. It shows that all mortars have the same sequence of attack.

At 1 and 2 years of observation, ettringite was found deposited in zones around the aggregates (Fig. 9), filling the transition space or the space created by the cracking due to the localized expansion. This situation is attributable to the secondary mineralization described by Bonen [27].

The bell-shaped distribution of ettringite across specimens can be attributable to ettringite decomposition beyond the surface. Ettringite is an unstable compound at pH values bellow 10.7 and its decomposition may be expected when the pH falls bellow this value [37]. The pH reduction in the pore solution may be caused by the pH control in the solution or by carbonation of the mortar. According to Diamond [38], ettringite deposition occurs toward the inside the carbonated layer in concretes exposed to sulfate bearing soils. However, small amounts of ettringite can be found in outer zone of a mortar.

4.3. Gypsum formation

When the alumina supplied by the AFm phase is deficient, ettringite crystallization ceases and the SO_4^{2-} react with Ca^{2+} initiating the gypsum crystallization [39]. Consequently, this reaction consumes Ca^{2+} from solution and more CH are decomposed into the pores causing CH depletion. In all profiles, it can be observed that gypsum was generally detected in the outer layers beyond the maximum distribution of ettringite. This sequence of reaction is typical in mortars containing AFm phase prior to sulfate immersion. The formation of gypsum causes the softening of the external layer of mortar while the interior of the matrix remains cohesive [39–41]. These observations agree with the type of deterioration reported in the visual appearance of all mortars after 1 year in sulfate solution.

As gypsum results from a CH substitution reaction, the amount of CH and its localization play a decisive role. At early hydration stages, precipitation of CH causes massive deposits of crystals on the paste–aggregate interface, which leads to the inevitable increase of porosity in this region. For PC and PLC10 mortars, massive gypsum formation around the aggregates was observed at 1 year (Fig. 10). Corrosion of edges and corners described in the visual assessment is also attributable to the gypsum formation in parallel veins to the sulfate attack front [27,29,30]. Bensted [42] suggests that the limestone filler grains modify the paste microstructure and that the topochemical growth of CH upon $CaCO_3$ crystals might occur and hence facilitate the access of SO_4^{2-} to form gypsum. Also, limestone filler increases the hydration rate of PC leading to the precipitation of CH located around the filler grains and the aggregate surfaces, but it does not have pozzolanic properties. Consequently, limestone filler does not produce C-S-H at later ages that consumes part of the CH, fills the pores, and improves the

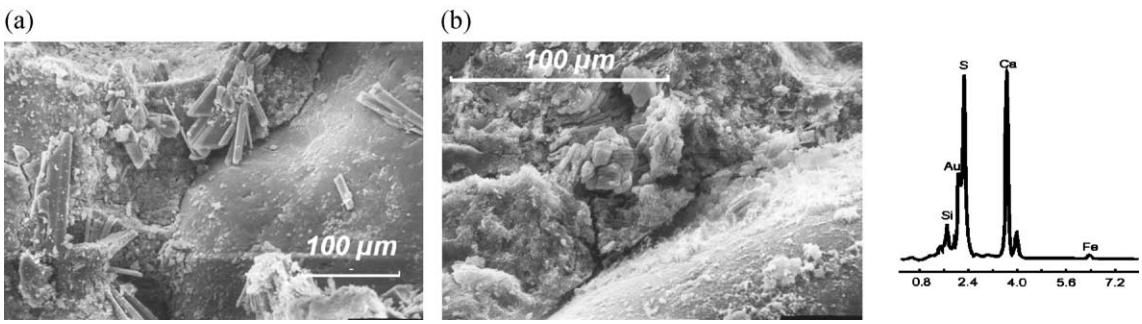

Fig. 10. SEM photographs of massive gypsum formation around the aggregates (a) PC mortar at 1 year and (b) PLC20 mortar at 1 year.

transition zone as other active addition (e.g., fly ash, silica fume, natural pozzolan).

In the corroded surface, the complete depletion of CH caused by gypsum formation is also accompanied with a deposition of calcium carbonate (calcite) crystals, which could cause a decrease in the amount of gypsum due to the decomposition of solid phases containing sulfate. For this degradation stage, mortar shows a dominant gypsum environment and the C-S-H will be affected reducing its intrinsic strength and stiffness [39,40].

4.4. C-S-H decalcification

In the outer transition zone, mortars contain little or no CH, and this compound is needed to preserve the integrity of C-S-H creating a surrounding environment with elevated pH. At the surface of PC paste, Gollop and Taylor [30] report that C-S-H is markedly decalcified after the complete dissolution of CH when it was exposed to Na_2SO_4 solution (0.25 mol/l). In profiles presented here, the CH is fully depleted and the gypsum environment was detected at several millimeters bellow the surface. Consequently, the decalcification of C-S-H could be expected causing modifications in its chemical and microstructural composition [38]. Decalcification of C-S-H depends on the depth and the area closer to the surface would have a higher degree of decalcification [27].

Hartshorn et al. [8] report that worst performance of pastes containing limestone filler is when they are immersed in $MgSO_4$ solution as opposed to Na_2SO_4 solutions. In $MgSO_4$ solution, decalcification and breakdown of C-S-H is more extreme due to the ingress of Mg^{2+} and the subsequent reaction to give a magnesium silicate hydrate [28]. Consequently, $MgSO_4$ attack may cause the C-S-H breakdown that provides the silica to favor the thaumasite formation in mortar containing limestone filler. This attack can also occur in low C_3A PC and blended PC containing large proportions of pozzolan, fly ash, silica fume, or slag [43,44].

4.5. Thaumasite formation

Finally, the scenario and the actors for the thaumasite-related damage are present. According to Collepardi [45], thaumasite may form from reaction of calcium carbonate, calcium sulfate, the C-S-H, and water. In Na_2SO_4 solution, decomposition of C-S-H appears to be the source of the reactive silica and this is available in the pore solution to react with the calcium carbonate from the limestone filler and the SO_4^{2-} from solution to form thaumasite.

Fig. 11a illustrates the alteration of microstructure near the surface (spalled zone) of PLC20 mortar after 2 years. SEM analysis shows a large amount of needle crystals up to 0.5 μm in diameter and up to 3–4 μm in length. EDS of these crystals is also shown in the Fig. 11 indicating the presence of calcium, silica, and sulfate. Traces of aluminum are also detected. Composition determined by this technique is very close to that of thaumasite. Fig. 11b shows crystals at 3–4 mm in depth in massive deposition containing silica and alumina in their EDS patterns indicating that thaumasite–ettringite crystals coexist as a limited solid solution [46] or that ettringite exerts a catalytic effect on thaumasite formation [47]. For the needle-like crystals observed in PC mortar, the EDS pattern showed only the presence of alumina in its composition. There is no evidence regarding thaumasite formation through the action of carbonation (dissolved CO_2 in solution) in this mortar.

Subsequently, the evidence of thaumasite formation as the final stage of sulfate attack in PLC is analyzed according to the main differences between ettringite and thaumasite formation reported by Collepardi [45].

(a) Ettringite causes expansion, but even after cracking the material still remains sound and cohesive. Conversely, thaumasite causes the mortar to become incoherent and nonresistant. These observations agree with the type of deterioration observed by visual assessment of PLC10 and PLC20 mortars, while the PC mortar bars expand maintaining theirs integrity.

(b) The presence of thaumasite is often preceded by the formation of ettringite. For all the cements used, XRD profiles show that ettringite was always detected at early ages. In the attack front, profile compounds also confirm that the deeper attack front is characterized by ettringite formation. The final stage is characterized by the presence of thaumasite in the outer surfaces. This situation will usually be the case for PC with high or moderate C_3A content as used in this experiment. These cements can

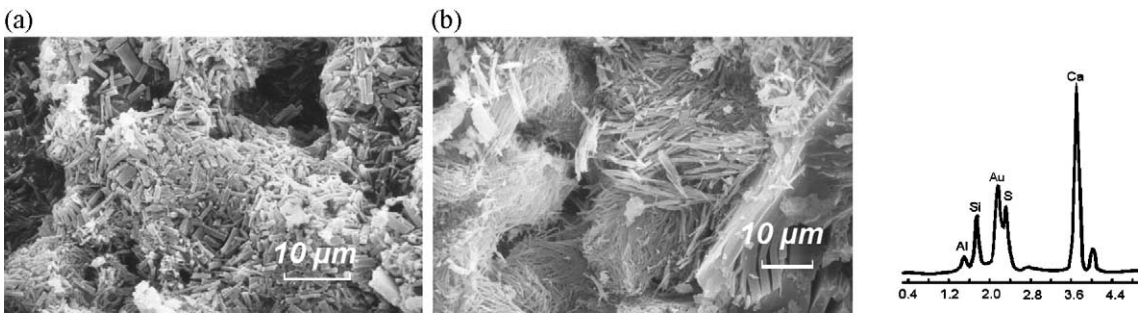

Fig. 11. SEM photographs thaumasite in PLC20 mortar after 2 years in sodium sulfate solution (a) near the surface and (b) mixed ettringite and thaumasite.

produce a lot of ettringite whose formation always precedes that of thaumasite. This situation could be different for low C_3A PC [3,16].

(c) Low temperatures favor the formation of both processes, especially that of thaumasite formation at around 5 °C and relative humidity of 90%. Bensted and Munn [35] and Bensted [48,49] affirm that thaumasite forms below 15 °C, especially at about 10 °C or less, ideally within the range 0–5 °C under cold, damp conditions. Also, this reaction does not occur in any perceptible extent at about 20 °C or above. However, Diamond [38] reports that significant contents of thaumasite have been found in buildings located in Southern California, a region with mild temperatures.

The XRD, SEM, and EDS analyses presented here on samples near the surface of mortars containing limestone filler confirm the presence of thaumasite at ambient temperature as the final stages of reaction. At low temperature, it is expected that this reaction will be more extended. Ludwig and Mehr [17] found that the formation of ettringite is decisive at 20 °C and thaumasite formation only occurred after long time of storage (600 days).

In this test, thaumasite formation could be favored by the pH control in the exposure solution. The decomposition of ettringite, the C-S-H decalcification, and the gypsum-dominant environment may be expected at this pH. All these conditions tend to promote and to preserve the formation of thaumasite. According to Gaze and Crammond [16], the thaumasite does not appear to form at pH below of 10.5. However, once formed, it can remain in contact with pH solutions as low as 7.

5. Conclusions

The following conclusion can be drawn:

1. Moderate C_3A PCs containing limestone filler were found more susceptible to sodium sulfate attack and less durable than the corresponding plain mortar as indicated by their larger expansions, greater surface deterioration, deeper transition zone of attack, greater deposition of gypsum, and higher degree of CH depletion.

2. The sulfate attack in mortars containing limestone filler is characterized by an inward movement of the reaction front leading first to the formation of ettringite, later to gypsum deposition, and finally to thaumasite formation when the decalcification of mortar leads to the breakdown of C-S-H providing reactive silica.

3. The reaction sequence in limestone filler cement is essentially the same as in the case of PC. The main difference is that, at later stages, thaumasite is formed from the decomposition of the ettringite first formed at ambient temperature.

4. Mortar with 20% of limestone filler is shown to be more permeable than the PC mortar according to the depth of sulfate transition zone at 1 year.

5. The deposition of ettringite and gypsum around the aggregates indicates the vulnerability of the paste–aggregate transition zone in limestone filler-blended cements to chemical attack.

Acknowledgements

Results presented in this paper are part of Project PICT97 12-00000-01323 sponsored by the Agencia Nacional de Promoción Científica y Técnica and the Secretaria de Ciencia y Técnica de la Universidad Nacional del Centro de la Provincia de Buenos Aires.

References

[1] BRE, Sulphate and acid resistance of concrete in the ground, Build. Res. Establ. Dig., Garston, UK 363 (1991).
[2] P.K. Mehta, Sulfate attack on concrete—a critical review, in: J. Skalny (Ed.), Mater. Sci. Concr., vol. III, American Ceramic Society, Westerville, USA, 1992, pp. 105–130.
[3] N.J. Crammond, M.A. Halliwell, The thaumasite form of sulfate attack in concretes containing a source of carbonate ions—a microstructural overview, Second CANMET/ACI International Symposium on Advances in Concrete Technology, Am. Concr. Inst. SP-154 (1995) 357–380.
[4] I. Soroka, N. Stern, Effect of calcareous fillers on sulphate resistance of portland cement, Bull. Am. Ceram. Soc. 55 (6) (1976) 594–595.
[5] G. Piasta, Z. Sawicz, G. Koprowski, Z. Owsiak, Influence of limestone powder filler on microstructure and mechanical properties of concrete under sulphate attack, Proc. 10th Int. Congr. Chem. Cem., Sweden (1998) (4iv018 8 pp.).
[6] J. Zelic, R. Krstulovic, E. Tkalcec, P. Krolo, Durability of the hydrated limestone–silica fume Portland cement mortars under sulphate attack, Cem. Concr. Res. 29 (6) (1999) 819–826.
[7] M.A. González, E.F. Irassar, Effect of limestone filler on the sulfate resistance of low C_3A Portland cement, Cem. Concr. Res. 28 (11) (1998) 1655–1667.
[8] S.A. Hartshorn, J.H. Sharp, R.N. Swamy, Thaumasite formation in Portland–limestone cement pastes, Cem. Concr. Res. 29 (8) (1999) 1331–1340.
[9] A. Brosoi, S. Collepardi, L. Copolla, R. Troli, M. Collepardi, Sulfate attack on blended portland cement, in: V.M. Malhotra (Ed.), Proceedings of the Fifth CANMET/ACI International Conference on Durability of Concrete, Barcelona, Spain, Am. Concr. Inst. SP-192, vol. I, 2000, pp. 417–432.
[10] F.M. Lea, The Chemistry of Cement and Concrete, Arnold, London, 1970.
[11] M. Venuat, Effet de certains paramètres sur l'essai de durabilité aux eaux sulfatées, Rev. Matér. Constr. 650 (1968) 376–381.
[12] C.F. Ferraris, J.R. Clifton, P.E. Stutzman, E.J. Garboczi, Mechanism of degradation of portland cement-based systems by sulfate attack, in: K.L. Scrivener, J.F. Young (Eds.), Mechanism of Degradation of Portland Cement-Based Systems, E&FN Spon, London, 1997, pp. 185–192.
[13] I. Biczock, Concrete Corrosion and Concrete Protection, Urmo Ed., Spain, 1968.
[14] P.W. Brown, An evaluation of the sulfate resistance of cements in a controlled environment, Cem. Concr. Res. 11 (5) (1981) 719–727.
[15] J.H.P. Van Aardt, The influence of temperatures on sulfate attack on portland cement mortars, Proc. 5th Int. Congr. Chem. Cem., Tokio III (1968) 250.

[16] M.E. Gaze, N.J. Crammond, The formation of thaumasite in a cement: lime:sand mortar exposed to cold magnesium and potassium sulfate solutions, Cem. Concr. Compos. 22 (3) (2000) 209–222.
[17] U. Ludwig, S. Mehr, Destruction of historical buildings by formation of ettringite and thaumasite, Proc. 8th Int. Congr. Chem. Cem, Brazil V (1986) 181–188.
[18] R.D. Hooton, Effects of carbonate additions on heat of hydration and sulfate resistance of portland cements, in: P. Klieger, R.D. Hooton (Eds.), Carbonate Additions to Cement, ASTM Spec. Tech. Publ., vol. 1064, 1990, pp. 73–81.
[19] E.F. Irassar, M. González, V. Rahhal, Sulphate resistance of Type V cements with limestone filler and natural pozzolan, Cem. Concr. Compos. 22 (5) (2000) 361–368.
[20] Y. Tezuka, D. Gomes, J. Martins, J.G. Djanikian, Durability aspect of cement with high limestone filler content, Proc. 9th Int. Congr. Chem. Cem., New Delhi, India V (1992) 53–59.
[21] A.P. Barker, D.W. Hobbs, Performance of Portland limestone cements in mortar prisms immersed in sulfate solutions at 5 °C, Cem. Concr. Compos. 21 (2) (1999) 129–137.
[22] Z. Sawicz, S.S. Heng, Durability of concrete with addition of limestone powder, Mag. Concr. Res. 48 (175) (1995) 131–137.
[23] P.F. McGrath, R.D. Hooton, Re-evalution of the AASHTO T259 90 days salt pounding test, Cem. Concr. Res. 29 (7) (1999) 1239–1248.
[24] N.J. Crammond, Quantitative X-ray diffraction analysis of ettringite, thaumasite and gypsum in concrete and mortars, Cem. Concr. Res. 15 (1985) 431–441.
[25] J.G. Wang, Sulfate attack on hardened cement paste, Cem. Concr. Res. 24 (4) (1994) 735–742.
[26] R.S. Gollop, H.F.W. Taylor, Microstructural and microanalytical studies of sulfate attack: III. Sulfate resistant Portland cement: Reaction with sodium and magnesium sulfate solution, Cem. Concr. Res. 25 (7) (1995) 1581–1590.
[27] D. Bonen, A microstructural study of the effect produced by magnesium sulfate on plain and silica fume-bearing Portland cement mortars, Cem. Concr. Res. 23 (3) (1993) 541–553.
[28] D. Bonen, M.D. Cohen, Magnesium sulfate attack on Portland cement paste: II. Chemical and mineralogical analyses, Cem. Concr. Res. 22 (4) (1992) 707–718.
[29] H.T. Cao, L. Bucea, A. Ray, S. Yozghatlian, The effect of cement composition and pH of environment on sulfate resistance of Portland cements and blended cements, Cem. Concr. Compos. 19 (2) (1997) 161–171.
[30] R.S. Gollop, H.F.W. Taylor, Microstructural and microanalytical studies of sulfate attack: I. Ordinary Portland cement paste, Cem. Concr. Res. 22 (6) (1992) 1027–1038.
[31] M.A. González, E.F. Irassar, Ettringite formation in low C_3A Portland cement exposed to sodium sulfate solution, Cem. Concr. Res. 27 (7) (1997) 1061–1072.
[32] C. Vernet, G. Noworyta, Mechanism of limestone fillers reactions in the system (C_3A-CSH_2-CH-CC-H), Proc. 9th Int. Congr. Chem. Cem., New Delhi, India (1992) 430–436.
[33] H. Kuzel, Initial hydration reactions and mechanisms of delayed ettringite formation in Portland cement, Cem. Concr. Compos. 18 (3) (1996) 195–203.
[34] V.L. Bonavetti, V.F. Rahhal, E.F. Irassar, Studies on the carboaluminate formation in limestone filler blended cements, Cem. Concr. Res. 31 (6) (2001) 8753–8859.
[35] J. Bensted, J. Munn, A discussion of the paper "Durability of the hydrated limestone—silica fume Portland cement mortars under sulphate attack" by Zelic, R. Krstulovic, E. Tkalcec, P. Krolo, Cem. Concr. Res. 30 (8) (2000) 1333–1334.
[36] H. Kuzel, H. Pöllmann, Hydration of C_3A in presence of $Ca(OH)_2$, $CaSO_4{\cdot}2H_2O$ and $CaCO_3$, Cem. Concr. Res. 21 (5) (1991) 885–895.
[37] A. Gabrisova, J. Havlica, Stability of calcium sulphoaluminate hydrates in water solutions with various pH values, Cem. Concr. Res. 21 (6) (1991) 1023–1027.
[38] S. Diamond, Microscopic Features of ground water induced sulfate attack in highly permeably concretes, in: V.M. Malhotra (Ed.), Proceedings of the Fifth CANMET/ACI International Conference on Durability of Concrete, Barcelona, Spain, Am. Concr. Inst. SP-192, vol. I, 2000, pp. 403–416.
[39] P.K. Mehta, Mechanism of sulfate attack on Portland cement concrete—another look, Cem. Concr. Res. 13 (3) (1983) 401–406.
[40] Rasheeduzzafar, Influence of cement composition on concrete durability, ACI Mater. J. 89 (6) (1992) 574–586.
[41] P.S. Mangat, J.M. Khatib, Influence of fly ash, silica fume, and slag on sulfate resistance of concrete, ACI Mater. J. 92 (5) (1993) 542–551.
[42] J. Bensted, A discussion of the paper: "Studies about a sulfate resistant cement: Influence of admixtures" by M.T. Blanco, S. Giménez, F. Puertas and T. Vazquez, Cem. Concr. Res. 25 (5) (1995) 1129–1130.
[43] O.S.B. Al-Amoudi, M. Maslehuddin, Effect of magnesium sulfate and sodium sulfate on the durability of plain and blended cements, ACI Mater. J. 92 (1) (1995) 15–24.
[44] R.D. Hooton, J.J. Emery, Sulfate resistance of a Canadian slag cement, ACI Mater. J. 87 (6) (1990) 547–555.
[45] M. Collepardi, Degradation and restoration of masonry walls of historical buildings, Mater. Struct. 23 (1990) 81–102.
[46] J. Bensted, Thaumasite a deterioration products of hardened cement structure, Cemento 85 (1) (1988) 3–10.
[47] M. Collepardi, Thaumasite formation and deterioration in historic buildings, Cem. Concr. Compos. 21 (2) (1999) 147–154.
[48] J. Bensted, Thaumasite—background and nature in deterioration of cements, mortars and concretes, Cem. Concr. Compos. 21 (2) (1999) 117–121.
[49] J. Bensted, Discussion of "Quantification of thaumasite in cementitious material by 29Si{1H} cross-polarization magic-angle NMR spectroscopy" by J. Skibsted, L. Hjorth and J. Jakobsen, Adv. Cem. Res. 9 (35) (1997) 135–138.